PAPER Nr. : 16

AN IMPROVED METHOD FOR THE COMPUTATION OF UNSTEADY TRANSONIC POTENTIAL FLOW - APPLICATION FOR AIRFOIL AND BLADE PERFORMANCE PREDICTION

BY

H. BEZARD, M. COSTES

Office National d'Etudes et de Recherches Aérospatiales
29, avenue de la Division Leclerc
Châtillon-sous-Bagneux (France)

FIFTEENTH EUROPEAN ROTORCRAFT FORUM

SEPTEMBER 12 - 15, 1989 AMSTERDAM

AN IMPROVED METHOD FOR THE COMPUTATION OF UNSTEADY TRANSONIC POTENTIAL FLOW - APPLICATION FOR AIRFOIL AND BLADE PERFORMANCE PREDICTION

H. BEZARD, M. COSTES

Office National d'Etudes et de Recherches Aérospatiales
29, avenue de la Division Leclerc
Châtillon-sous-Bagneux (France)

Summary

A finite difference code solving the Unsteady Full Potential equation for both 2D and 3D flows has been improved by introducing a C-grid topology. The results are compared to previous calculations performed with an H-grid. An important effort to calculate the airfoils and blades inviscid drag has been undertaken. The different ways to estimate the unsteady inviscid drag (pressure drag, wave drag) are discussed, and the method is applied to airfoils and blades performance evaluation.

I. INTRODUCTION

The flow field around helicopter rotor blades presents many different features during the blade rotation, such as transonic effects on the advancing blade side, high angle of attack and low speed flows on the retreating side, strong interactions between the blade and the wake system. Since these complex phenomena are difficult for a single computational method to handle at a reasonable cost, specific algorithms adapted to compute efficiently a part of these phenomena were developed, the full rotor flow being obtained by coupling different methods together.

At the Aerodynamics Department of ONERA, a part of the activity has been devoted to compute the transonic flow on the advancing blade side. For most of the practical cases shock wave strength remains moderate and therefore Potential methods were developed first. Their advantages compared to Euler methods are a good cost efficiency and robustness. On the other hand, the calculated pressure jump across shock waves is not correct and the irrotational flow implies the use of an external wake model. Nevertheless, Potential methods constitute a good compromise between computer cost and accuracy and therefore are suitable for practical design.

Steady Potential methods are widely used for airfoil design using numerical optimisation techniques [1]. They have allowed to design a new generation of efficient helicopter airfoils at ONERA. A step forward could however be achieved by using unsteady methods which might allow the conception of new helicopter airfoils. As far as three-dimensional flows are concerned, an Unsteady Transonic Small Disturbance approximation to the Potential Equation has been successfully used to generate efficient blade tips which reduce the amount of supercritical flows [2]. Nevertheless, the Small Disturbance approximation cannot provide a correct description of the leading edge flow and therefore an accurate rotor performance prediction.

A finite difference code solving the Unsteady Full Potential Equation was also developed to compute the transonic flow appearing around helicopter rotor blades. This method, called FP3D, is able to compute both 2D and 3D flows and a good correlation with experiment or with other computed results has been found [3, 4]. However, in order to use this method for practical design, important improvements have to be made both in accuracy and efficiency. An important step in this direction can be achieved by choosing a more well-adapted grid topology than the previous H-grid. A good compromise between accuracy and efficiency can be obtained using a C-grid topology.

In a first part of the paper, the FP3D method will be described. Then the improvements obtained with the new C-grid for 2D and 3D configurations will be shown. In a third part of the paper, the methods to evaluate the unsteady wave drag

will be discussed and, at last, applications of the method for unsteady performance prediction of airfoils and blades will be presented. Future improvements to obtain an efficient design tool will also be discussed.

II. Computational method

The FP3D code solves the Unsteady Full Potential Equation with a finite difference algorithm written in a generalized coordinates system. It was developed by ONERA and the US Army Aeroflightdynamics Directorate within the framework of a MOU. The system of equations solved is the mass conservation equation and the Bernoulli equation, which can be written in generalized coordinates:

$$\frac{\partial}{\partial \tau}\left(\frac{\rho}{J}\right)+\frac{\partial}{\partial \xi}\left(\frac{\rho U}{J}\right)+\frac{\partial}{\partial \eta}\left(\frac{\rho V}{J}\right)+\frac{\partial}{\partial \zeta}\left(\frac{\rho W}{J}\right)=0$$

$$\rho=\left\{1+\frac{\gamma-1}{2}\left[-2\,\Phi_{\tau}-(U+\xi_t)\Phi_{\xi}-(V+\eta_t)\Phi_{\eta}-(W+\zeta_t)\Phi_{\zeta}\right]\right\}^{1/\gamma-1}$$

ρ is the fluid density, U, V and W are the velocity components along the ξ, η and ζ directions, and J is the Jacobian of the transformation which maps the space into the ξ, η and ζ coordinates. For two-dimensional flows, only two space derivatives along the ξ and ζ directions are retained. A density and fluxes linearization by a Taylor expansion versus the velocity potential gives a fully implicit equation in conservation form. The density and metric terms are exactly calculated at mid-cell for an accurate fluxes computation. Stability is maintained in supercritical regions by an upwind density biasing. Non reflecting boundary conditions are written at the grid boundaries to allow perturbations to get out of the computational domain. The equation is solved using an approximate factorization technique to obtain a set of simple tridiagonal systems to compute.

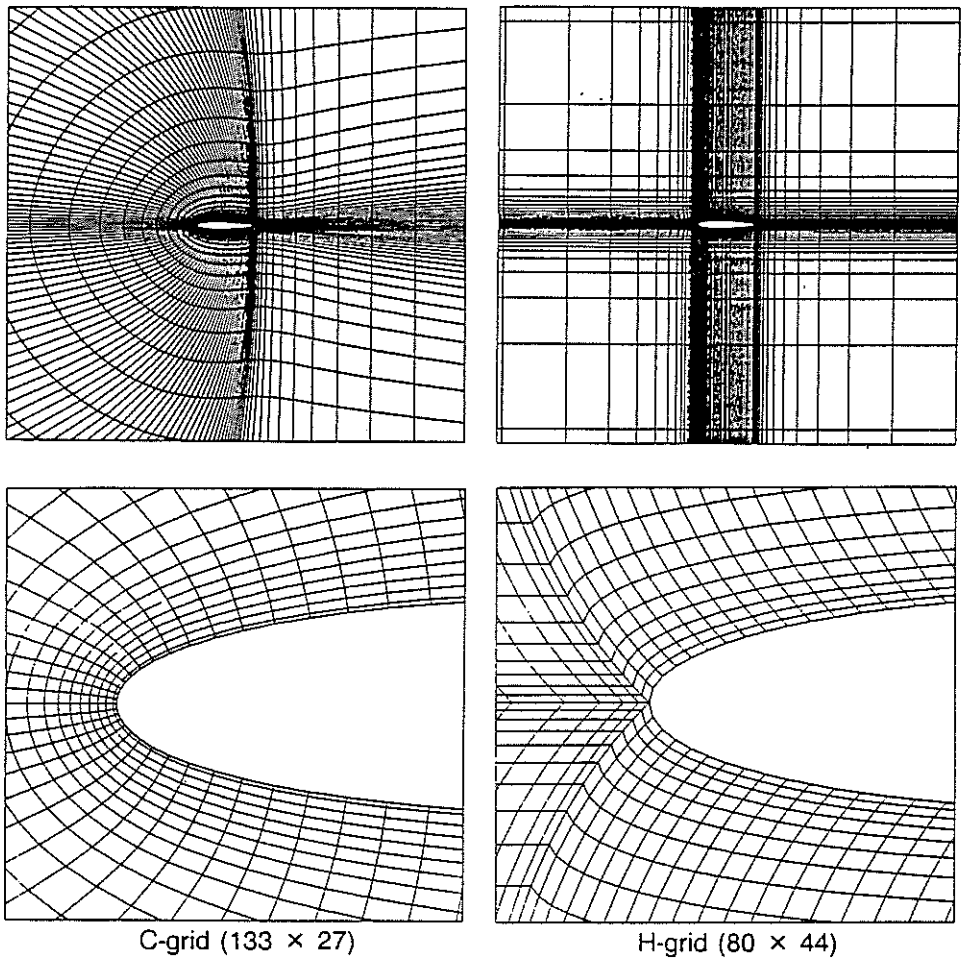

C-grid (133 × 27) H-grid (80 × 44)

Fig. 1 - Grid topology comparisonNACA 0012 - 3500 mesh points, 100 points on airfoil surface.

The FP3D code was initially written for an H-grid topology. This topology is the simplest one to implement because the grid lines are close to a natural coordinates system. However, such a grid leads to a non-optimal points distribution since local grid refinements extend towards the grid boundaries. Furthermore, the leading edge region is poorly represented and the grid is singular there, with an important distortion. These comments are illustrated in figure 1. Comparatively, a C-grid topology provides a better grid points distribution in space and a smooth and regular representation of the blade leading edge. Furthermore, the grid boundaries match the computational boundaries (airfoil surface and wake, outer boundaries), which provides a better computational efficiency. The 2D and 3D versions of the FP3D code were therefore rewritten for a C-grid topology. As shown on figure 1, the grid is at mid-cell inside the blade surface to implement the boundary conditions easily. The computation is implicit across the wake were the upper and lower grids overlap. A special problem arise beyond the blade tip for three-dimensional cases, because a singularity is present when gridding a zero thickness airfoil. Figure 2 shows how the problem was removed. Like in the wake, the upper and lower grids overlap there, and the computation is implicit across the cut. At the grid "leading edge", this implies a quadratic interpolation along the ζ grid lines. Thanks to the C-grid topology, the new coding was much simplified since boundary conditions are only applied at the grid boundaries and it results in a more efficient code.

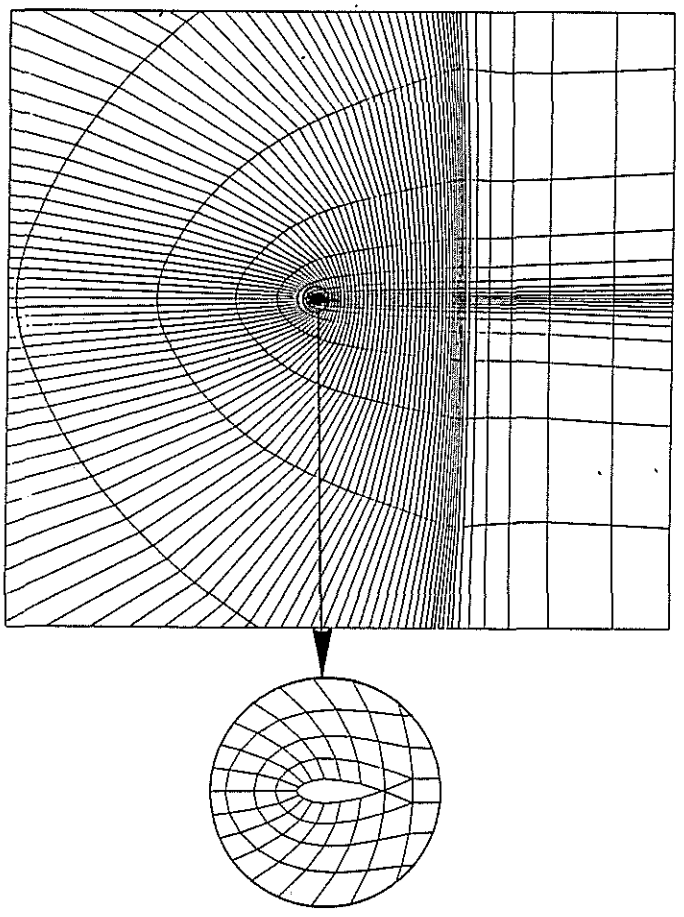

Fig. 2 - C-grid off the blade.

III. H-grid and C-grid results comparison

III.1. 2D Case

The comparison is made on a lifting case already presented by F.X. Caradonna [5] and simulating the real flow conditions encountered on helicopter rotor blades. The rotor has a NACA 0012 airfoil, an aspect ratio of 13.7, a forward speed of 220 km/h, an advance ratio of 0.25 and the 0.925 R station is computed. At this station, the upstream 2D conditions are a sinusoidal variation of the angle of attack given by the law $\alpha = 2.75° - 3.25° \sin \psi$ and a local Mach number variation given by : $M = 0.670 + 0.181 \sin \psi$.

Calculations have been carried out on the two different grid topologies of section II with the same number of points in the mesh (3 500 points) and on the airfoil surface (100 points).

Figure 3 shows the influence of the grid topology on the unsteady pressures. The C-grid solution gives an important improvement, especially at the leading edge: the stagnation pressure is much more accurate and for the retreating blade side the suction peak is more realistic. This leads to a higher lift coefficient for the retreating blade side (Figure 4) combined with an important decrease of the pressure drag coefficient, which is a real improvement although this term should be nearly zero for this part of the rotor disk.

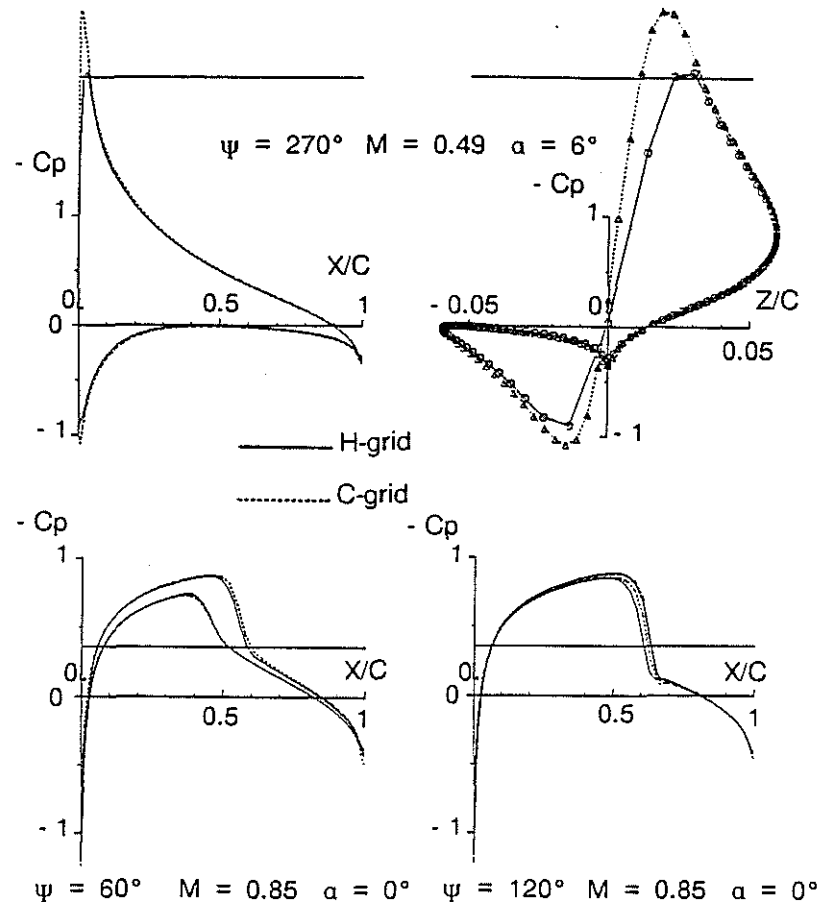

Fig. 3 - Influence of grid topology on unsteady pressures (2D case)
V_0 = 220 km/h, μ = 0.25, y/R = 0.92, NACA 0012.

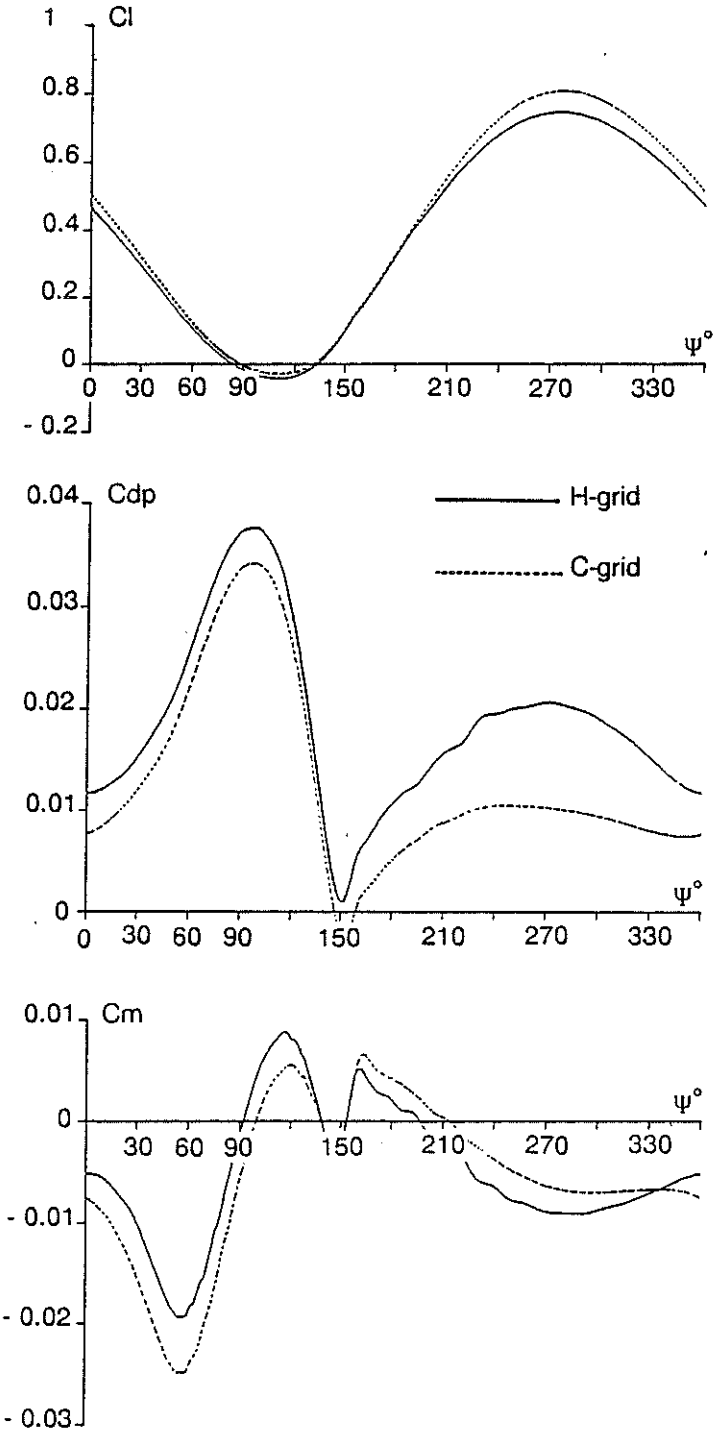

Fig. 4 - Influence of grid topology on aerodynamic coefficients (2D case)
V_o = 220 km/h, μ = 0.25, y/R = 0.92, NACA 0012.

For the advancing blade side, shock waves have slightly stepped back to the trailing edge with the C-grid solution (Figure 3) which causes a decrease of the moment coefficient (Figure 4), but their strength is not really affected by the grid modification.

The use of a C-grid has also provided a reduction in computing time of about 20 % (on CRAY XMP-18) and a better calculation robustness.

III.2. 3D Case

The new FP3D version has also been applied to three-dimensional configurations. The wake is modelled by a vortex wake code written by Aérospatiale and called METAR. As for the 2D case, the better code efficiency has allowed a 20 % computer time reduction. The calculated case is a model rotor which was tested in the ONERA S2Ch wind tunnel. The rotor has rigid blades with PF1 tip shapes; its aspect ratio is 6.97. The test case is a relatively high speed case with a rotating tip Mach number of 0.61 and an advance ratio of 0.4; the thrust coefficient C_T/σ is equal to 0.075. The model tested had a cyclic pitch control device and the cyclic law was $\theta_{1S} = \beta_{1C}$ and $\beta_{1S} = 0$.

The comparison between the C-grid and H-grid versions has been made with approximately the same number of grid points:

- $121 \times 22 \times 14$ for the C grid, with 95 points on each blade section
- $70 \times 22 \times 24$ for the H grid, with 90 points on each blade section.

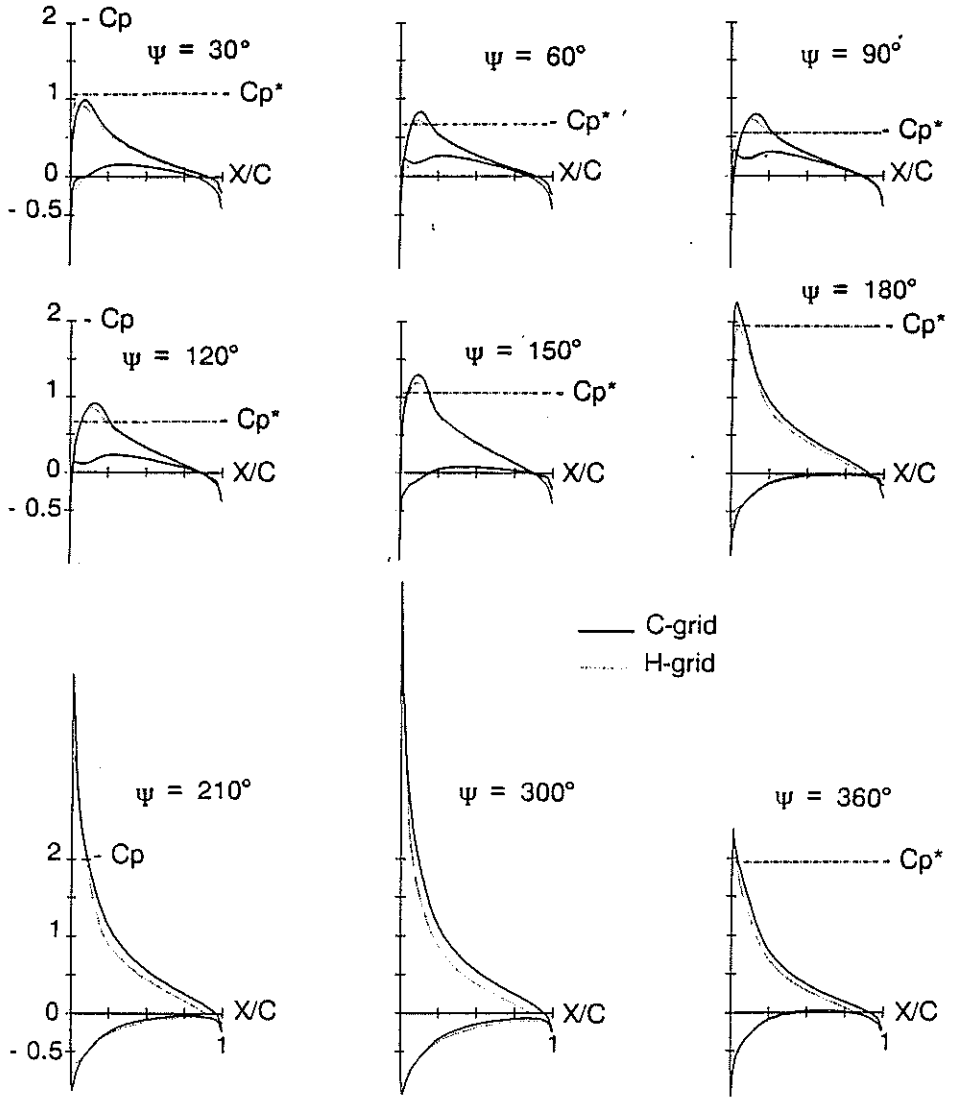

Fig. 5 - PF1 blade, $C_T/\sigma = 0.075$, $\mu = 0.4$, $M_{\Omega R} = 0.61$.

Figure 5 presents the computed results for a spanwise section y/R = 0.85. The comments given for a 2D configuration are still true. The C-grid result provides a better description of leading edge flows (stagnation pressure and velocity peak) and the differences observed are more important for the retreating blade side. Compared to the experiment (Figures 6 and 7), the C-grid gives a better correlation than the H-grid. For the advancing blade side, however, the computed velocity is underestimated on the blade upper surface; a finer grid would probably improve the results. Finally, a discrepancy clearly appears between computation and experiment at the azimuth ψ = 360°. It can be seen for both C-grid and H-grid calculations and might be due to the influence of the rotor hub wake. This local discrepancy is also obvious on the C_N evolution versus the azimuth (Figure 8). This figure shows the better correlation of the C-grid results with experiment. However, for azimuthes between 240° and 330°, the computed lift is too high, and the discrepancy increases for the inboard sections of the blade. This can probably be explained by the occurrence of important viscous effects due to high angle of attack flows.

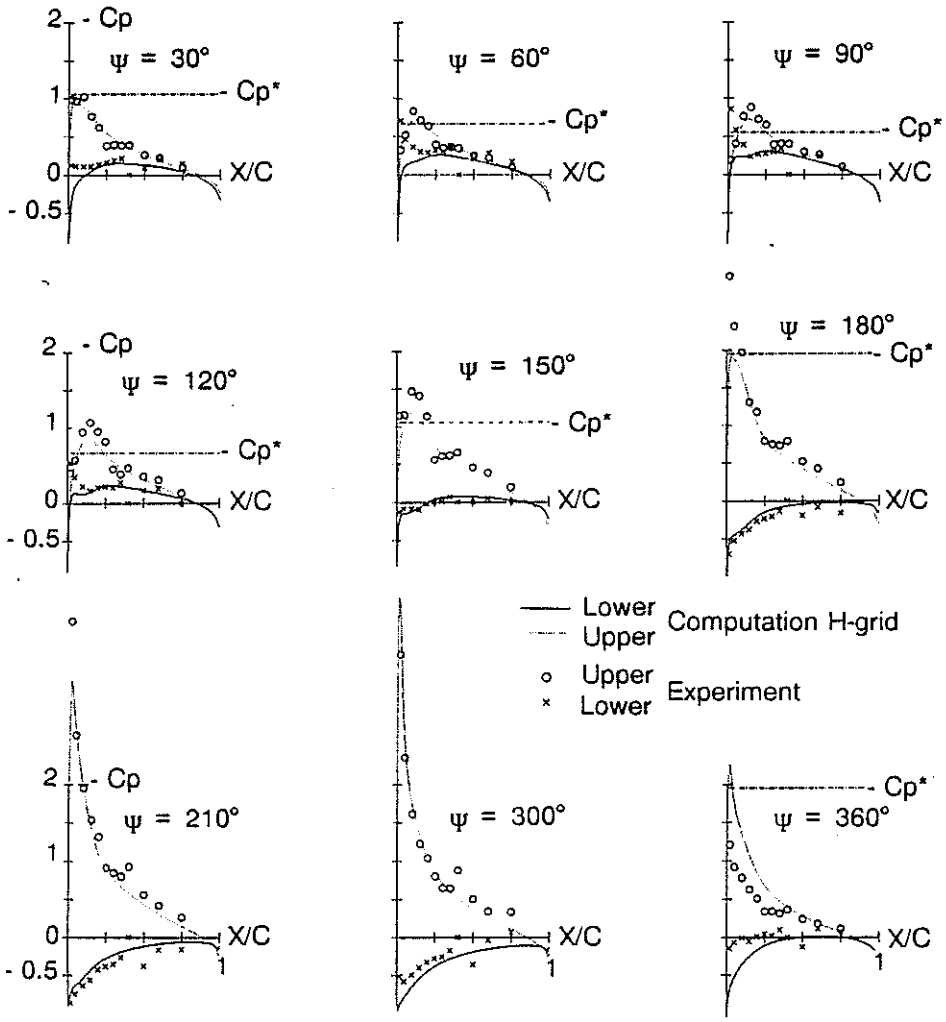

Fig. 6 - PF1 blade, C_T/σ = 0.075, μ = 0.4, $M_{\Omega R}$ = 0.61.

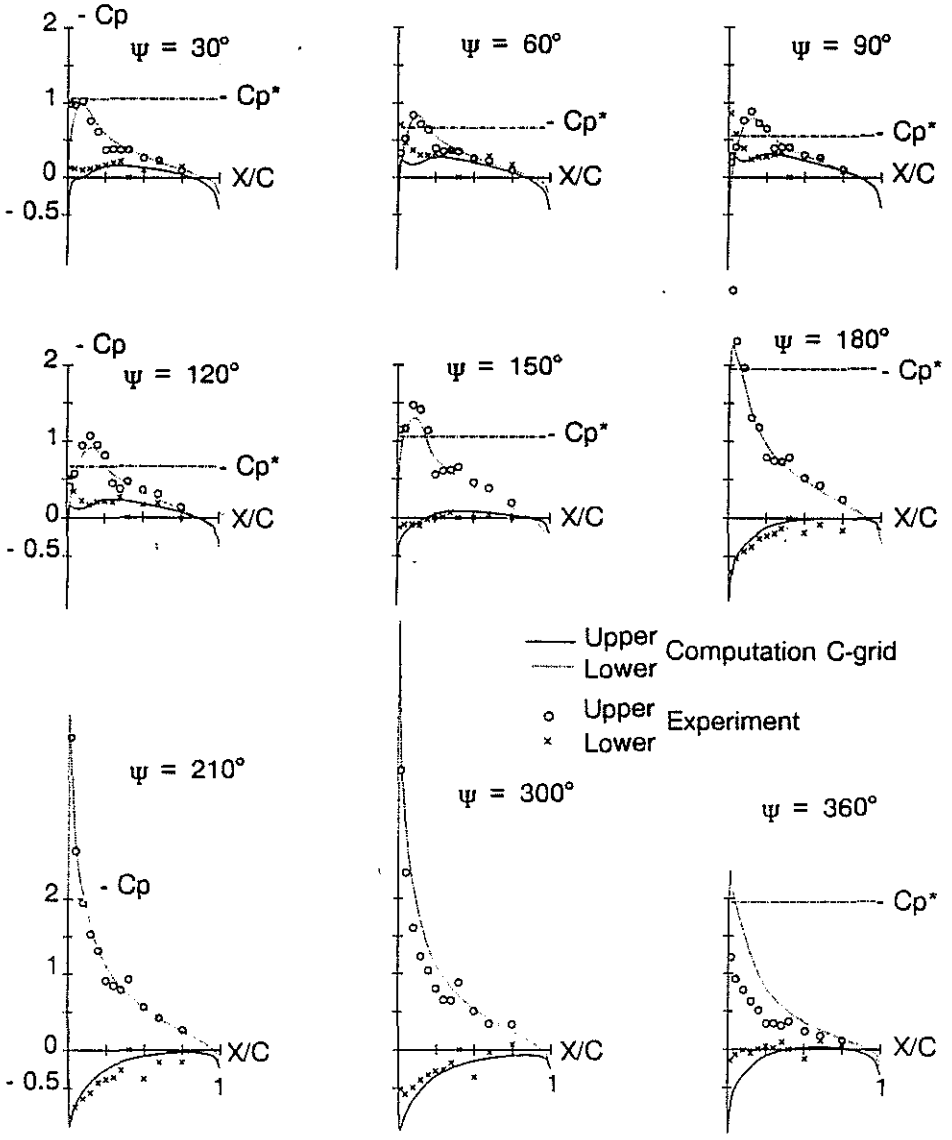

Fig. 7 - PF1 blade, $C_T/\sigma = 0.075$, $\mu = 0.4$, $M_{\Omega R} = 0.61$.

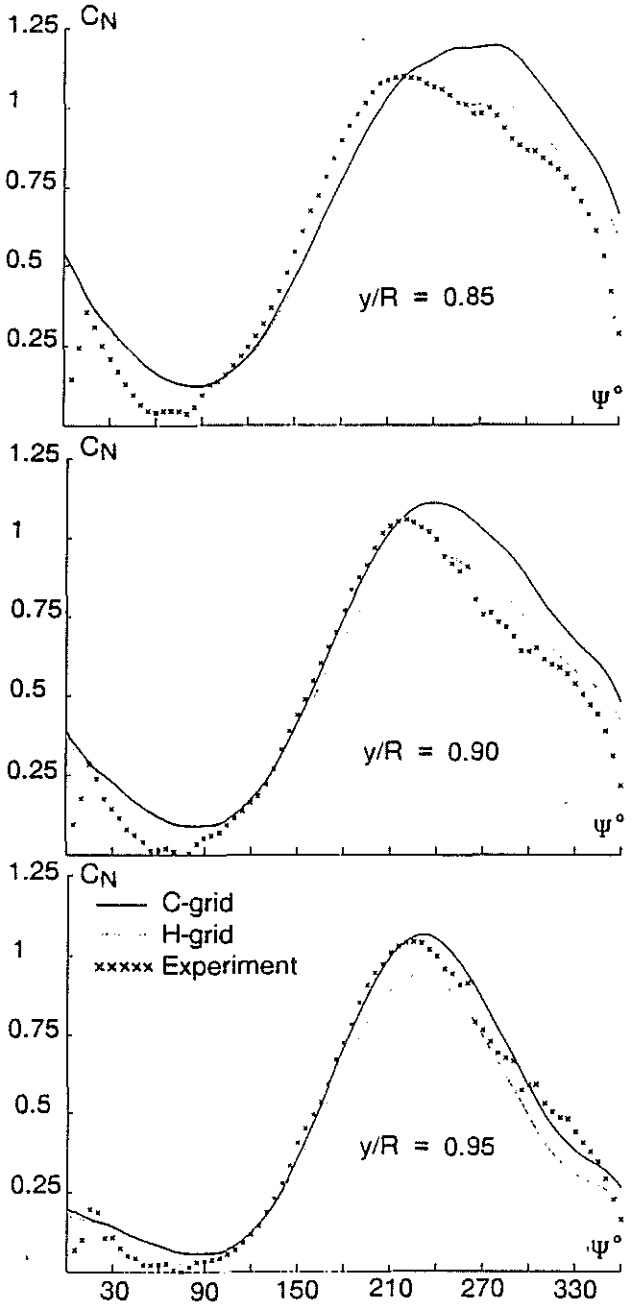

Fig. 8 - Evolution of the lift coefficient - PF1 blade
C_T/σ = 0.075, μ = 0.4, $M_{\Omega R}$ = 0.61.

These comparisons have shown the benefits given by the C-grid solution which provides better results for a lower cost. This is an important step to build a valuable code for helicopter performance prediction.

IV. Evaluation of the unsteady wave drag (2D case)

IV.1. Drag Evaluation by Pressure Integration

Figure 9 presents the evolution of the unsteady pressure drag coefficient for the OA 209 airfoil for which the oscillating Mach number and angle of attack simulate the conditions of a high speed forward flight (y/R = 0.88, V_0 = 350 km/h, μ = 0.45). Two pressure distributions are also shown: one for the advancing blade side with the presence of shock waves on the upper and the lower surfaces, and one for the retreating blade side with a high suction peak near the leading edge. It can be seen that the drag

coefficient for the retreating blade side can be higher than the drag for the advancing blade side although it should be nearly equal to zero without any shock waves on the airfoil.

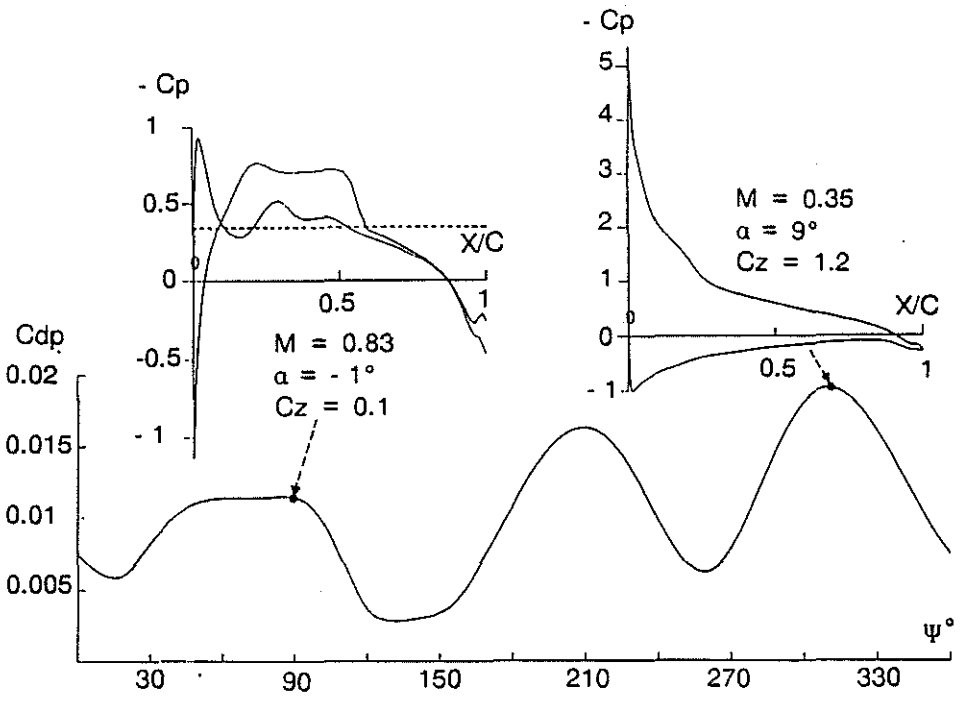

Fig. 9 - Unsteady pressure drag coefficient (2D case)
V_O = 350 km/h, μ = 0.45, y/R = 0.88, OA 209.

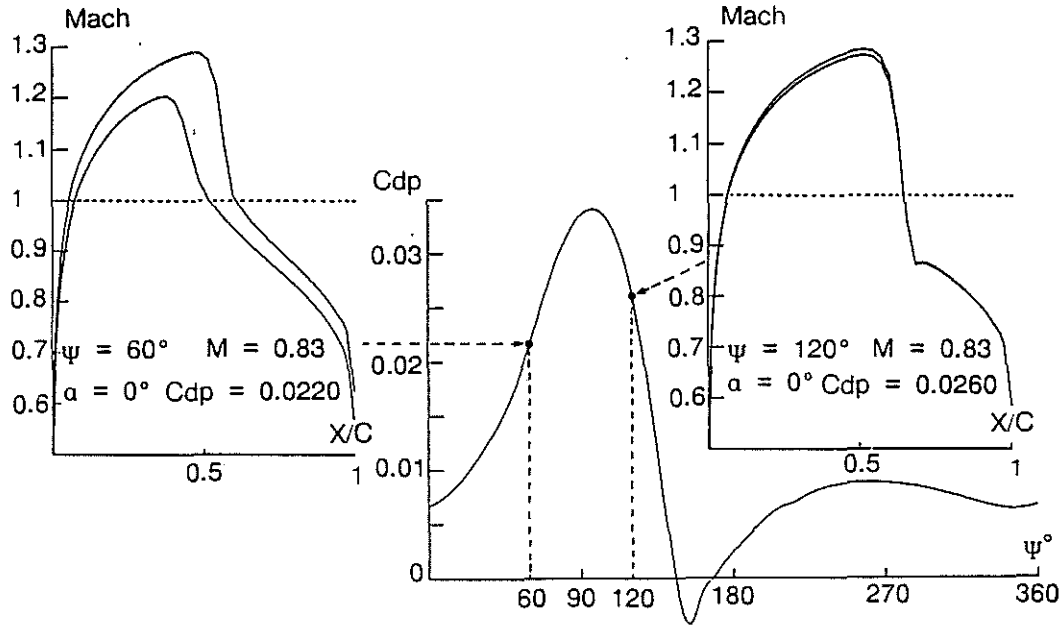

Fig. 10 - Unsteady pressure drag coefficient (2D case)
V_O = 220 km/h, μ = 0.25, y/R = 0.92, NACA 0012.

Another example of the inaccuracy of pressure integration for drag estimation is given on figure 10 for the case already shown in section III.1. Mach number distributions are shown for azimuthes 60° and 120° where the upstream Mach number and angle of attack are identical. The flow unsteadiness is clearly pointed out there with very different shock wave intensities and positions. However, the pressure drag

coefficients are very close with only 18 % variation. Making a quasi-steady assumption, one can estimate the wave drag using Lock formula [6]:

$$Cd_W = 0.243 \left(\frac{1 + 0.2\,M_\infty^2}{M_\infty} \right)^3 \frac{(M_{10} - 1)^4 (2 - M_{10})}{M_{10}(1 + 0.2\,M_{10}^2)} \frac{1}{K_W}$$

where M_{10} is the Mach number on the airfoil surface just ahead of the shock, K_W is the local airfoil curvature and M_∞ is the upstream Mach number. This formula gives $Cd_W = 0.0255$ for $\Psi = 60°$ and $Cd_W = 0.0422$ for $\Psi = 120°$ (65 % variation), which seems more reasonable.

The main reason for the inaccuracy in pressure drag prediction is the low number of mesh points used in the calculations (3 500 points). Increasing the mesh density would of course improve the solution but several authors [7, 8, 9] show that more than 20 000 mesh points are needed to obtain a good evaluation of the pressure drag, which is very prohibitive in computer time.

So another method to compute the drag has been studied.

IV.2. Unsteady Wave Drag Evaluation

Considering a control surface S bounded by a curve C surrounding shock waves and supported by the airfoil surface. Then, using the momentum theorem projected in the upstream direction (x-axis), the drag D is given by:

$$D = \int\int_S \frac{\partial \rho U}{\partial t}\, dxdz + \int_C (\rho\, U\, V_n + p\, n_x) ds \tag{1}$$

where V_n is the normal component of the velocity on the boundary of the control surface.

In order to reduce numerical errors due to the use of artificial viscosity in the supersonic regions of the flow, it is interesting to substract the continuity equation multiplied by U_∞:

$$\int\int_S U_\infty \frac{\partial \rho}{\partial t}\, dxdz + \int_C \rho\, U_\infty V_n\, ds = 0 \tag{2}$$

and using :

$$\int_C p_\infty n_x\, ds = 0 \tag{3}$$

The drag is given by:

$$D = \int\int_S \left(\frac{\partial \rho U}{\partial t} - U_\infty \frac{\partial \rho}{\partial t} \right) dxdz + \int_C \left| \rho\,(U - U_\infty) V_n + (p - p_\infty) n_x \right| ds$$

The drag coefficient Cd_W can be expressed with the non-dimensional values $\tilde{U} = U/a_\infty$, $\tilde{\rho} = \rho/\rho_\infty$, $\tilde{t} = t.a_\infty/L$, and using $p/\rho^\gamma = cste$:

$$Cd_W = \overbrace{\frac{2}{M_\infty^2} \int\int_S \left(\frac{\partial \tilde{\rho} \tilde{U}}{\partial \tilde{t}} - M_\infty \frac{\partial \tilde{\rho}}{\partial \tilde{t}} \right) dxdz}^{Cd_{W_1}}$$

$$+ \overbrace{\frac{2}{M_\infty^2} \int_C \left\{ \tilde{\rho}(\tilde{U} - M_\infty)\tilde{V}_n + \frac{\tilde{\rho}^\gamma - 1}{\gamma} n_x \right\} ds}^{Cd_{W_2}} \tag{4}$$

The first term Cd_{W_1} in the formula is a pure unsteady term which can be either positive or negative according to the sign of the momentum variations.

The second part Cd_{W_2} is always positive and represents the flow characteristics at a given time. With some assumption, this term gives the approximate formula seen in section IV.1.

From a theoretical point of view, the choice of the control surface S needed to calculate the equation (4) does not matter, except that the boundary must surround shock waves, but in practice, due to numerical errors introduced by the artificial viscosity the results are affected by this choice.

Figure 11 shows three unsteady wave drag calculations with the same conditions (test case) but with three different control surfaces: the first one has a constant size and stretches from the leading edge to the trailing edge of the airfoil, the second one fits all the supersonic zone while the third one fits shock waves very closely. For practical considerations, all the boundaries lean on mesh lines.

Both terms of the expression (4) are presented on figure 11 for the airfoil upper side. A constant size control surface S_1 does not seem to be a reasonable choice because it gives irrealistic values for the unsteady drag term. On the other hand, the results concerning the control surfaces S_2 and S_3 are quite satisfactory; this is illustrated by the fact that the calculation gives a zero wave drag coefficient for a supersonic zone without any shock wave (retreating blade). Furthermore, according to the discussion in section IV.1, the second part of the wave drag formula (4) must give a higher value for $\Psi = 120°$ than for $\Psi = 60°$ because of stronger shock waves for the second azimuth angle. It is the case for the control surface S_3 (see figure 11) but not for surfaces S_1 and S_2. Afterwards, wave drag calculations will be carried out with the control surface S_3 which extends on the airfoil surface from the point where the local Mach number is maximum up to the last supersonic point. This surface has the same height than the supersonic zone.

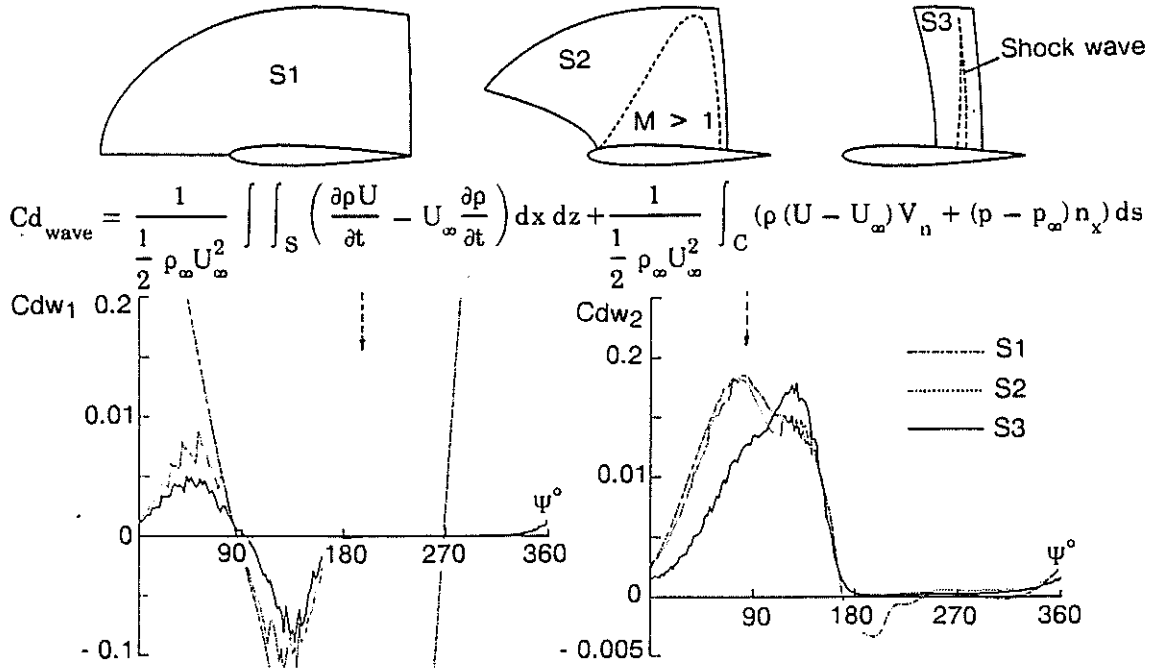

Fig. 11 - Unsteady wave drag coefficient (2D case)
V_O = 220 km/h, μ = 0.25, y/R = 0.92, NACA 0012 (upper side).

Figures 12 and 13 show the different terms of the expression (4) and a comparison with the pressure drag coefficient for the two cases of section III.1. The pure unsteady term Cdw_1 (Figure 12) is very large and high negative values can be obtained in the second quadrant ($90° \leq \psi \leq 180°$) when the upstream Mach number is decreasing. This explains why the large dissymmetry observed on the local Mach number distributions for $\psi = 120°$ (see section IV.1) does not lead to a large deviation for the unsteady wave drag. Figure 13 shows that the evolutions of the wave drag and pressure drag coefficients are quite close for the advancing blade side although the corresponding drag levels are quite different.

Consequently, drag evaluation by pressure integration is not an accurate tool for airfoil performances prediction. However, it can give qualitative results and therefore can constitute a first approach to evaluate rotor blade performances. This is particularly important for 3D flows for which wave drag evaluation is complex and difficult to implement.

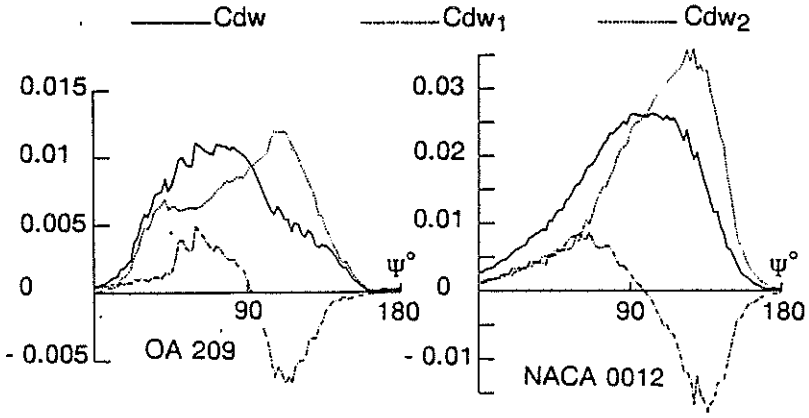

Fig. 12 - Unsteady wave drag coefficient (2D case) (advancing blade).

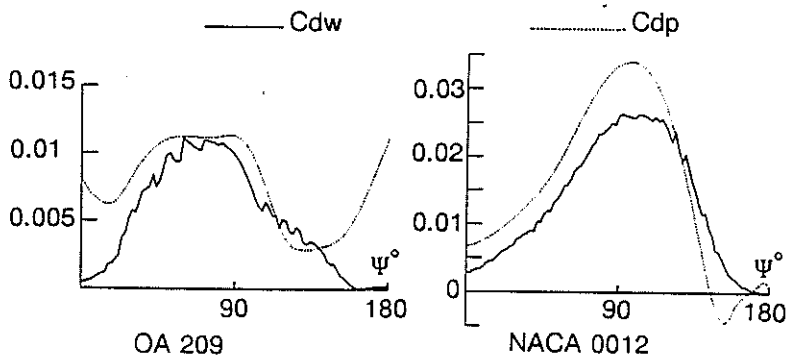

Fig. 13 - Wave drag and pressure drag comparison (2D case) (advancing blade).

V. Unsteady performances prediction

V.1. Airfoils

V.1.1. Steady flow

In 2D steady flows, rotor blade airfoils are generally classified through two main parameters: the maximum lift coefficient at a given Mach number (usually 0.4) and the drag divergence Mach number (Mdd) at zero lift.

A code solving the Potential flow equation is not able to give the maximum lift coefficient which is a pure viscous phenomenon, but it can provide a drag divergence Mach number which is accurate enough to make a ranking of different airfoils. Figure 14 shows a comparison between calculation and experiment (made at ONERA) for three 12 % thickness to chord ratio rotor blade airfoils. The experimental values of Mdd are always higher than the calculated ones, due to viscous effects, but the relative differences between the various airfoils are nearly the same for the experiment and the calculation. This example shows that the program can accurately rank airfoils with different steady drag characteristics but cannot yet give an exact estimation of their real performances.

Mdd (Cl=0.)	Airfoil No.1	Airfoil No.2	Airfoil No.3
Calculation	0.746	0.763	0.768
Experiment (ONERA)	0.780	0.790	0.796

Fig. 14 - Drag divergence Mach number at zero lift.

V.1.2. Unsteady prediction

For 2D unsteady flows, airfoil performances can be evaluated considering average forces per period. This can be written in a general form:

$$\overline{F} = \frac{1}{2\pi} \int_0^{2\pi} F \, d\psi \qquad \text{where} \qquad F = \frac{1}{2} \rho L C V^2$$

Then the corresponding mean aerodynamic coefficients are:

$$C = \frac{F}{\frac{1}{2} \rho L V^2} \quad \text{which gives} \quad \overline{C} = \frac{1}{2\pi \overline{M}^2} \int_0^{2\pi} C M^2 \, d\psi.$$

For a given flight configuration, the variation of the upstream Mach number is known and gives the term $\overline{M}^2$. Different airfoils can be compared then in term of the mean wave drag ($\overline{Cdw}$) for a same mean lift ($\overline{C\ell}$). Figure 15 shows a comparison between the same three airfoils for the evolution of the lift coefficient ($\overline{C\ell} = 0.4$) seen in section III.

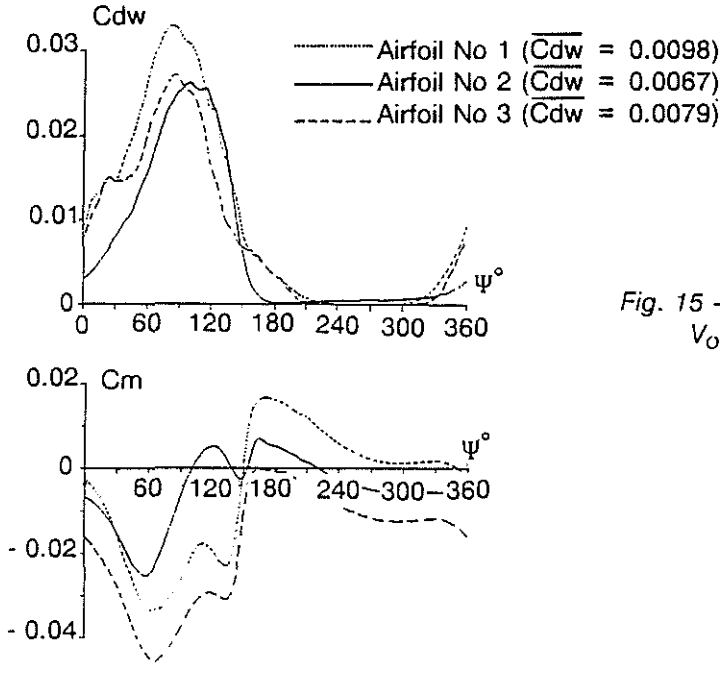

Fig. 15 - Airfoil comparison at iso mean lift ($\overline{Cl} = 0.4$)
V_O = 220 km/h, μ = 0.25, y/R = 0.92.

The mean wave drag coefficients are also given and for this configuration the second airfoil has the best unsteady performances, which was not the case for a steady evaluation.

This example shows that a rotor blade airfoil design using unsteady criteria would certainly give very different results than those obtained with classical steady methods. The present method associated with a boundary layer code will be used at ONERA in a numerical optimization process to define new improved airfoils.

V.2. Rotor blades

The FP3D code has been used to compare the performances of several blade tip shapes. The performance criterion chosen is the blade torque based on pressure integration. As mentioned in section IV, this integration does not give an accurate drag prediction but it can allow to compare several blades together.

The computed case is a very high speed case with a rotating tip Mach number of 0.64 and an advance ratio of 0.5. Since our goal is to compare several blade tip shapes to reduce transonic effects on the advancing blade side, the configuration is nonlifting. The computed blades are a rectangular blade, a 30° aft swept blade (F30), a forward swept blade (F - 30) and a blade with a parabolic swept tip (PF2). Figure 16 shows the computed iso-Mach lines for the azimuthes 60°, 90° and 120° and it shows the well-known following result: the F30 blade reduces transonic effects in the first quadrant, while the same effect can be seen in the second quadrant for the F-30 blade. This is also the case all along the advancing side of the rotor disk for the PF2 blade. When looking at the computed torque (Figure 17), this effect is obvious. The torque maximum value for the F30 tip is slightly reduced and shifted forward when compared to the rectangular blade, while it is shifted backward for the F - 30 tip blade. The maximum torque values are nearly the same for the F30 and F - 30 blades. This figure also shows the important improvements brought by the PF2 tip shape. When integrating the torque versus the azimuth, one finds that the torque reduction is equal to 8 % for the F - 30 blade, 15 % for the F30 blade and 36 % for the PF2 blade.

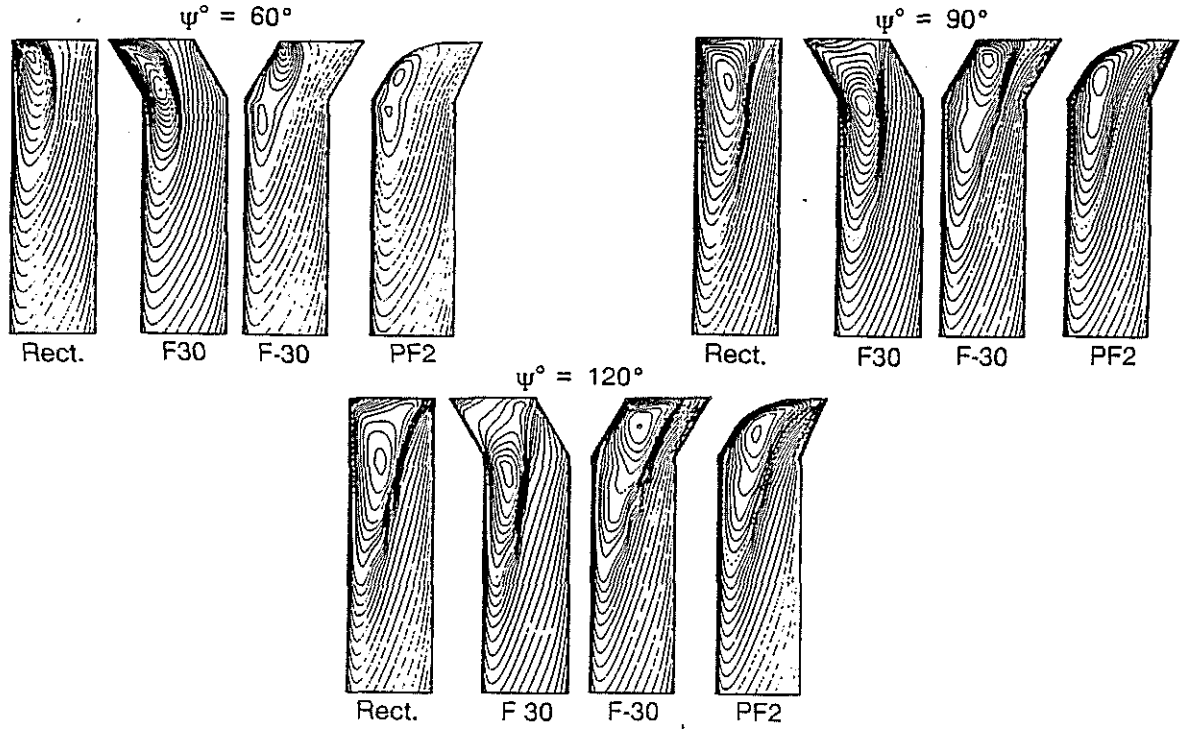

Fig. 16 - Iso-Mach lines. Nonlifting case.
μ = 0.5, $M_{\Omega R}$ = 0.64, NACA 0011.

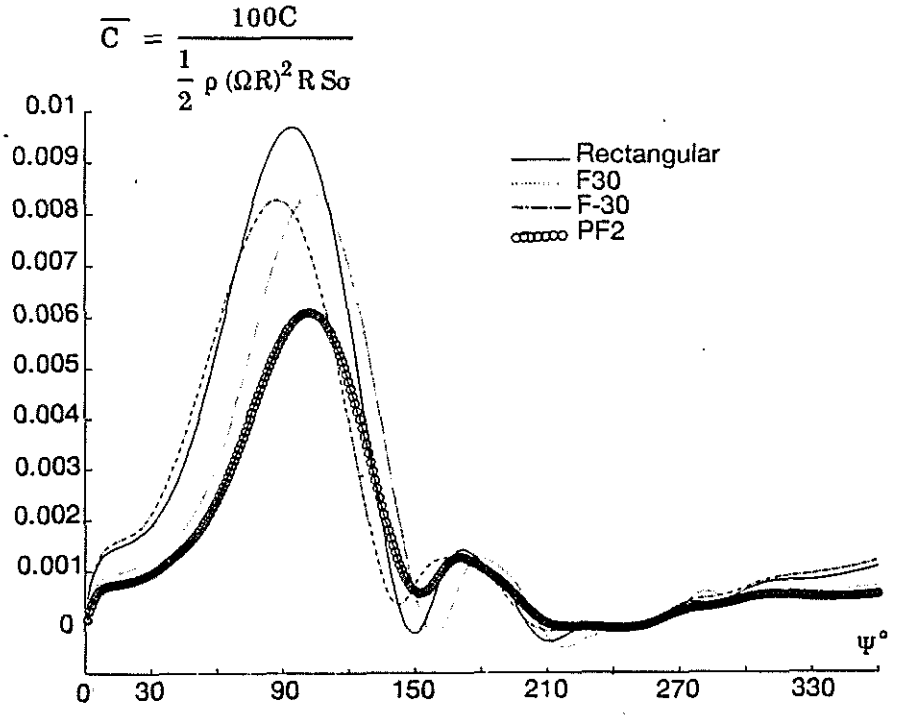

Fig. 17 - Torque evaluation by pressure integration (0.61 R → R). Nonlifting case. μ = 0.5, $M_{\Omega R}$ = 0.64.

This example shows how the method can be applied for blade design. However, further efforts must be undertaken to be able to compute the rotor performances accurately. The method described in section IV to compute the wave drag in 2D flows will be applied to three-dimensional configurations, and the FP3D code will be coupled with an unsteady three dimensional boundary layer code (weak coupling) to compute the viscous drag.

VI. Conclusion

In this paper were presented the last improvements concerning an unsteady transonic potential flow code used for rotor blades and airfoils calculation. The change from a H-grid topology to a C one allowed a great improvement of the computed results in the leading edge area (stagnation pressure and velocity peak), in the code robustness and in the computer time for both 2D and 3D applications.

A 2D unsteady wave drag evaluation has been carried out by integrating the momentum equation over a control surface which surrounds shock waves. This evaluation showed that the pure unsteady effect is important. This drag evaluation and the classical pressure drag are close for the advancing blade side.

Calculations made on different airfoils or different blade tips allowed to classify them by their relative unsteady performances. The criteria used then were the mean wave drag value per period for the 2D case and for the 3D case the torque calculated by integration of the 2D pressure drags along the blade. The results obtained showed that the present method can be used for rotor blades and airfoils design.

In order to predict more accurately the real aerodynamic performances, a boundary layer code will be added to the present potential method (weak coupling) and the wave drag evaluation will be extended to the 3D case.

Moreover, the 2D method will be used in a numerical optimization process to define new airfoils with unsteady specifications.

REFERENCES

[1] Reneaux, J., Thibert, J.J., "The use of numerical optimization for airfoil design", AIAA 3rd Applied Aerodynamics Conference, Colorado Springs, October 14-16, 1985.

[2] Desopper, A., "Study of the unsteady transonic flow on rotor blades with different tip shapes", 10th European Rotorcraft Forum, The Hague, August 28-31, 1984 and Vertica, Vol. 9, (3), 1985.

[3] Costes, M., Jones, H.E., "Computation of transonic potential flow on helicopter rotor blades", 13th European Rotorcraft Forum, Arles, September 8-11, 1987.

[4] Costes, M., Desopper, A., Ceroni, Ph., Lafon, P., "Flow field prediction for helicopter rotor with advanced blade tip shapes using CFD techniques", 2nd Int. Conf. on Basic Rotorcraft Research, College Park, February 16-18, 1988.

[5] Caradonna, F.X., "The flow over a helicopter blade tip in the transonic regime", Vertica, Vol. 2, 1978, p. 43-60.

[6] Lock, R.C., AGARD lecture series on "Drag prediction and reduction", AGARD R-723.

[7] Viviand, H., "Numerical solutions of 2D reference test cases", AGARD Report 211, 6.1-6.68, 1985.

[8] Barton, J.T., Pulliam, T.H., "Airfoil computation at high angles of attack; inviscid and viscous phenomena", AIAA Paper 84-0524, 1984.

[9] Lerat, A., Sidès, J., International Conference on "Numerical Methods for Fluid Dynamics", Oxford University, March 21-24, 1988.